Investigation of energy absorption performances of a 3D printed fiber-reinforced bio-inspired cellular structure under in-plane compression loading

Fatemeh Ghorbani[1], Hussain Gharehbaghi[1], Amin Farrokhabadi[*1], Amir Bolouri[2], Amir Hossein Behravesh[1], Seyyed Kaveh Hedayati[1]

[1] Department of Mechanical Engineering, Tarbiat Modares University, Tehran, Iran.

[2] School of Engineering, University of the West of England, Bristol, UK.

[3] Additive Manufacturing Laboratory, Faculty of Mechanical Engineering, Tarbiat Modares University, Tehran, Iran

Abstract

This paper proposes glass-fiber-reinforced bone-inspired cellular structures to enhance energy absorption capability. The elastic modulus of the bone-inspired unit cell is obtained analytically based on the energy method and then employed in Particle Swarm Optimization (PSO) algorithm to get optimized cellular structures. In the optimized cellular structure, the stiffness is optimized and the energy absorption capacity is investigated. A Fused Filament Fabrication (FFF) 3D printing process is used to fabricate the cellular structures with continuous glass fiber-reinforced Polylactic acid (PLA). In-plane compression tests are performed to investigate the mechanical performance of cellular structures. Finite Element Modelling (FEM) is conducted to analyzed the mechanical performance of the structures. In FEM, the failure criterion is determined using the maximum stress and VUSDFLD subroutine, and the damage growth is modelled by decreasing the mechanical properties. A good agreement between numerical and experimental results was observed. Results demonstrated that the energy absorption in glass-fiber-reinforced PLA is ~250% higher than in the un-reinforced structure. The optimized cellular structure exhibits a stable prolonged plateau stress region and very high specific energy absorption parameters.

[*] Corresponding Author, Email Address: amin-farrokh@modares.ac.ir

Keywords: Fiber reinforced cellular structure; FFF 3D printing; Optimization; Energy absorption

Nomenclature

U	Strain energy
l'	Strut length
L	Unit cell height
W	Unit cell width
D	Unit cell depth
t	Strut thickness
β	Strut angle
h	Ply height
b	Ply width
l	Ply length
F	Axial force
M	Axial moment
m	Mass
A	Cross section area
E	Elastic modulus
E_s	Base material elastic modulus
E_c	Elastic modulus of the composite material
E_m	Elastic modulus of the matrix
E_f	Elastic modulus of the fiber
E_{ii}	Elastic modulus in the local coordinate system
V_f	Fiber volume fraction
I	Moment of inertia
I_{ii}	Second moment of inertia
ε_{ii}	Strain components
σ_{ii}	Stress components
ε_{ii}^0	Midplane strain components
κ_{ii}^0	Curvatures of the reference surface
z	Midline curvature
N_i	Force resultants
M_{ii}	Moment resultants
F_i	Axial forces in the local coordinate system
SEA	Specific Energy Absorption
CLE	Crush Load Efficiency
MCL	Mean Crushing Load
d_{max}	Maximum crushing displacement
$v_{ij}(k)$	Velocity of the particle in the k-th iteration
$x_{ij}(k)$	Position of the particle in the k-th iteration
ω	Inertia weight
r_i	Independent random function
c_i	Learning factor

1. Introduction

During several centuries, researchers are presented different 2D and 3D cellular structures to get structures with low weight and high strength. These structures consist of a periodic unit cell pattern in the in-plane directions. Cellular structures are commonly used in different applications through their exceptional mechanical properties. They can be utilized in various fields such as aerospace, biomedical engineering, transportation, and civil engineering [1]–[3]. Today 3D printing technology is provided to fabricate complex geometrical structures with relatively low-cost [4]–[7].

Various studies have assessed cellular structures intending to improve strength-to-weight ratio and stiffness [8], [9]. Also, researchers have investigated the energy absorption capability of cellular structures and enhanced this parameter to get applicable structures [10], [11]. Some of these studies modified the geometry of cellular structures and others suggested adding a second phase to the cellular structure as the reinforcement to enhance stiffness and energy absorption capacity [8], [12]. In this regard, Ingrole et al. [13] proposed a novel auxetic-strut structure with better mechanical properties than honeycomb and re-entrant auxetic structures. Results demonstrated that the compressive strength of the auxetic-strut structure is ~300% more than that of the honeycomb and ~65% more than that of the re-entrant auxetic structures. Gharehbaghi et al. [14] presented a novel lattice structure created by adding struts to the surface-based unit cell. They performed numerical simulations and experimental tests to assess the mechanical performance of the proposed structure. Results demonstrated that adding struts increased the energy absorption by about 106%, but the amount of force decreased significantly after reaching peak force. Okubo et al. [15] evaluated the effect of the irregularity of the lattice

structures on energy absorption properties. The lattice structures were designed using a three-dimensional Voronoi partitioning method, and the irregularities of the structures were controlled by the Voronoi seed point distribution. Lattice structure samples were fabricated by powder bed fusion with PA12 powder. Quasi-static compression loading was applied to assess the mechanical performance of lattice structures. The results demonstrate that irregular lattice structures with controlled coefficient variation are isotropic and absorb energy more than random lattice structures designed without planning. Ghazlan et al. [16], [17] have introduced a novel cellular structure inspired by trabecular bone. They investigate the novel cellular structure's mechanical properties and energy absorption experimentally and numerically. Their results demonstrated that the mechanical behavior of the novel structure is higher than conventional honeycomb and re-entrant auxetic structure. Wen et al. [18] have studied the crushing resistance and energy absorption performance of a novel pomelo peel-inspired honeycomb under out-of-plane and in-plane crushing numerically and experimentally. Results indicated that the specific energy absorption (SEA) and equivalent plateau stress for the proposed honeycomb structure improved by 1.5 (out-of-plane crushing) and 2.5 times (in-plane crushing) than that of conventional honeycomb. Ha et al. [19] presented a new bio-inspired hierarchical circular honeycomb (BHCH), mimicking the hierarchical structures from wood. The structure's mechanical properties and energy absorption were investigated under quasi-static compression tests and finite element (FE) analysis. The experimental results indicated that the BHCH has a higher specific energy absorption than the corresponding CH with the same wall thickness and the same volume of honeycombs. Xu et al. [20] have assessed the in-plane compressive behavior and energy absorption capability of a novel hybrid cellular structure consisting of re-entrant and hexagonal honeycomb unit cells. They conducted their studies using theoretical, finite element simulation, and experimental methods. Results showed that a novel hybrid cellular structure improved the mechanical properties significantly than re-

entrant and honeycomb structures. Doodi and Gunji [21] developed a novel hybrid type of lattice structure that is inspired by nature's structures. The lattice structures are designed based on some overlapping areas. The unit cells developed with different overlapping areas and wall thicknesses in a constant volume. Specimens were fabricated using the principle of stereolithography (SLA) technique. Compression testing was conducted to evaluate the energy absorption of the structures, and by comparing the results the best cellular structure in energy absorption is selected. Lu et al. [22] studied the out-of-plane dynamic crash behaviors of anti-tetrachiral, hexachiral, and hierarchical chiral structures and concluded that the anti-tetrachiral structure has higher plateau stress and energy absorption than hexachiral structures and can be employed as a good energy absorber structure. Zhang et al. [23] proposed a novel quadri-arc multi-cell honeycomb and employing the finite element method, the novel structure's dynamic behavior and energy absorption properties under in-plane impact loadings were investigated. Results indicated that the quadri-arc multi-cells significantly enhance the plateau stress by 45.8% and energy absorption by 56.3% under quasi-static simulations. Dawei et al. [24] investigated mechanical behavior and energy absorption capability of the uniform and graded structure of strut-based and surface-based gyroid in TPMS. Results showed that the surface-based gyroid structure has better energy absorption than the strut-based gyroid structure, and cellular structures with large gradients demonstrate better energy absorption capacity than those with a small gradient. Higuera et al. [25] have studied the mechanical properties and energy absorption of thermoplastic sheet gyroid structures and compared them with current materials. A compression test was performed to investigate their behavior. Their results showed that the structure's volume fraction and cell size could significantly affect peak and plateau stress regions, which generates higher specific energy absorption capacity. Wang et al. [26] studied the mechanical behaviors of polymeric TPMS sheets experimentally under quasi-static compression loading. Six different configurations including Schwarz Primitive, Schoen

Gyroid, Skeleton, Schoen I-WP, Schwarz Diamond, and P-W Hybrid were fabricated utilizing the fused filament fabrication (FFF) technique with polylactic acid (PLA) polymer. Results showed that among investigated structures a P-W Hybrid has the highest mechanical performance in energy absorption capacity, and a Schwarz Primitive has the lowest performance in energy absorption capabilities. Forés-Garriga et al. [27] extended research on the mechanical performance of three-dimensional lightweight cellular solids, including open-cell and closed-cell lattice structures and triply periodic minimal surfaces (TPMS), with different cell sizes and infill densities. Their experimental results indicated that Shell-TPMS designs are the most efficient cellular pattern, followed by the Skeletal-TPMS and the lattice structures.

Some studies proved that using multi-materials in the 3D printing process can be effective in improving mechanical properties. Rahman et al. [28] have numerically investigated the mechanical properties and energy absorption ability of hybrid (soft-hard) structures with gradient lattices. The results indicated that changes in the unit cell size show more energy absorption and mechanical performance; also, the combination of soft and hard materials provides the maximum energy absorption and stiffness in lattice structures. The main challenge of this study is the complexity of manufacturing samples with the combination of bi-material. Huang et al. [29] introduced a novel dual architecture phase lattice (DPL) structure consisting of hard and soft phases. Quasi-static compression tests and numerical simulations are conducted to study the deformation patterns and stress-strain responses. Their results revealed that introducing appropriate agreements of reinforcement phases can result in 112% and 37% increments for the compression strength and specific energy absorption, respectively. Rajendra et al. [30] assessed the honeycomb structure made of two different materials to introduce a structure with the highest EA capacity. They fabricated the honeycomb structure as a uniform material and two, three, and five layers, with two different materials. All samples are fabricated

using PolyJet 3D-printing technology and subjected to a compression test. Their results indicated a honeycomb structure with 5 different layers of the material has the best performance for energy absorption application.

Also, adding fibers is introduced to enhance the mechanical performance of the structures. On this point, Quan et al. [31] studied the in-plane mechanical properties of the re-entrant auxetic honeycomb structure, which is reinforced with continuous Kevlar fiber under compression loading. Results revealed that continuous fibers increase compressive stiffness and energy absorption by 86.3% and 100%, respectively. Veisi et al. [32] developed an analytical model to investigate the mechanical properties of the composite re-entrant structure based on classical lamination theory (CLT). They compared their results with experimental tests in previous studies. Results indicated that the proposed analytical model shows good agreement with experimental tests. Farrokhabadi et al. [33] studied the energy absorption capacity of the continuous fiber-reinforced re-entrant structure. They performed compression tests in both hollow and foam-filled structures. Results showed that the absorbed energy increases significantly by using foam, but the lack of control in foam injection inside the samples is one of the most important challenges of this research. Liu et al. [34] presented two types of polymeric periodic hybrid (PPH) structures with hexagonal and re-entrant unit cells. All the specimens were made by 3D printing technology using polylactic acid (PLA) material, and some hollow spaces were filled with PVC foam. They investigated the mechanical performance of the cellular structures numerically and experimentally. Results showed that PPH structures with foam filling in re-entrant cells exhibit higher elastic modulus and peak stress than those with foam filling in hexagonal cells. Farrokhabadi et al. [35] investigated the mechanical properties of the fiber-reinforced cruciform unit cell analytically and numerically under tensile loading. They evaluated their results using experimental tests. Results demonstrated that the in-plane elastic stiffness of the honeycomb is increased by about 60% using glass fiber.

Furthermore, Farrokhabadi et al. [36] developed an analytical model to estimate the mechanical properties of the fiber-reinforced U-type unit cell. They used experimental tests under tensile loading to validate the proposed theoretical model. Results showed that by employing continuous fiber, the stiffness is increased twice that without fiber structures in both x and y directions. Hao et al. [37] studied the mechanical properties and failure modes of 3D printed fiber-reinforced polyamide 12 (PA12) lattice structures utilizing the digital image correlation (DIC) technique. Their results demonstrated that adding glass fibers improved the mechanical properties and energy absorption ability of the composite lattice structures. Xin et al. [38] employed the discontinuous fibers to improve the specific energy absorption (SEA) of a carbon/epoxy composite tube by 51% under quasi-static uniaxial compressive loading. Hu et al. [39] investigated the mechanical properties of novel chiral composites with chopped carbon fiber (CF) as the reinforcement. The obtained results revealed that these structures have significant potential in the evolution of high-performance mechanical metamaterials. Plocher and Panesar [40] studied the influence of the intensity of grading on the compressive stiffness, energy absorption, and structural response in short fiber reinforced functionally graded lattice structures. Their results showed that the moderate grading of the density improved the total stiffness of the lattices significantly. Gunaydin et al. [41] investigated the compression behavior of the re-entrant and honeycomb structures. For each structure, three different materials were used, including Nylon, Carbon fiber-reinforced Nylon, and Glass fiber-reinforced Nylon. The FFF technique made all the samples and tasted them experimentally under quasi-static loading conditions. This study found that a multi-material approach enhanced the mechanical performance of the re-entrant cellular structures, such as specific energy absorption, compressive strength, and modulus over the single Nylon structure by 60%, 104%, and 201%, respectively. Also, lesser improvements of 15%, 60%, and 127% were observed for the hexagonal cellular structure in the same sequence.

The main aim of this study is to propose continuous fiber-reinforced cellular structures by conducting an optimization algorithm. Energy absorption capacity is considered the key parameter for assessing optimized structures and comparing them with a baseline structure. The proposed research consists of three parts. The first is related to an optimization algorithm. The equivalent mechanical properties for a bone-inspired unit cell were developed in the previous study [42] and their accuracy is validated. By employing the developed equations in the optimization algorithm, the optimized structures were achieved. The second part of the research involved fabricating samples with the FFF technique and then subjected to quasi-static compression loading. The other part of the research is finite element analysis employing the VUSDFLD subroutine to assign the mechanical properties to the composite material. Based on the foundation results, the conclusion was composed on the influence of the proposed topology optimization and employing fiber reinforcement on the energy absorption capacity. The present study's methodology can effectively be employed for designing energy absorber structures in automotive, aerospace, and biotechnology applications. It should be noted that composite materials have high strength and low energy absorption capability due to their fragility, so they could not be a good candidate for use in automobile components. By employing the cellular structures, while the weight of components is optimized, the amount of energy absorption is increased significantly, so these structures have a high potential to use in automobile components in overset and dangerous accident situations. Fig.1 illustrates using cellular structure in A-pillar and B-pillar. The requirement to reduce weight in the automotive industry to manage energy consumption well and the commitment to use recoverable materials in the design of parts increases the importance of the current study.

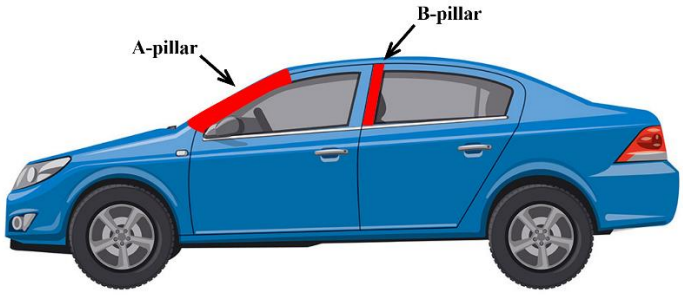

Figure 1. A-pillar and B-pillar in an automotive

1. Configuration of the baseline structure

The unit cell considered in this study has been inspired by the cancellous bone according to [17]. The cancellous bone structure has a porous area that displays different cellular structure patterns, including concave, convex, or hybrid cells. The bone-inspired cellular structure is introduced based on the hybrid design of cancellus bone and contains two different sub-cells, according to Fig. 2. The main purpose of this creation is to propose a unit cell with lower weight and higher energy absorption compared to traditional cellular structures [16].

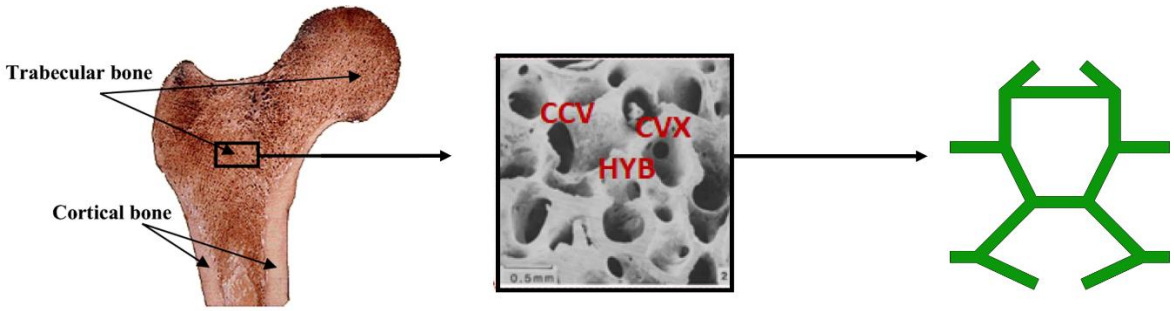

Figure 2. Cancellous bone structure [42]

The tessellation configuration and representative unit cell are shown in Fig.3a and 3b. The thickness of horizontal struts is double compared to diagonal struts. This occurs due to the limitations in the manufacturing of specimens. Geometrical parameters of the composite bone-inspired unit cell with 20mm×20mm×20mm dimensions are presented in Table1. The structure shown in Fig.3a was made to study energy absorption capability.

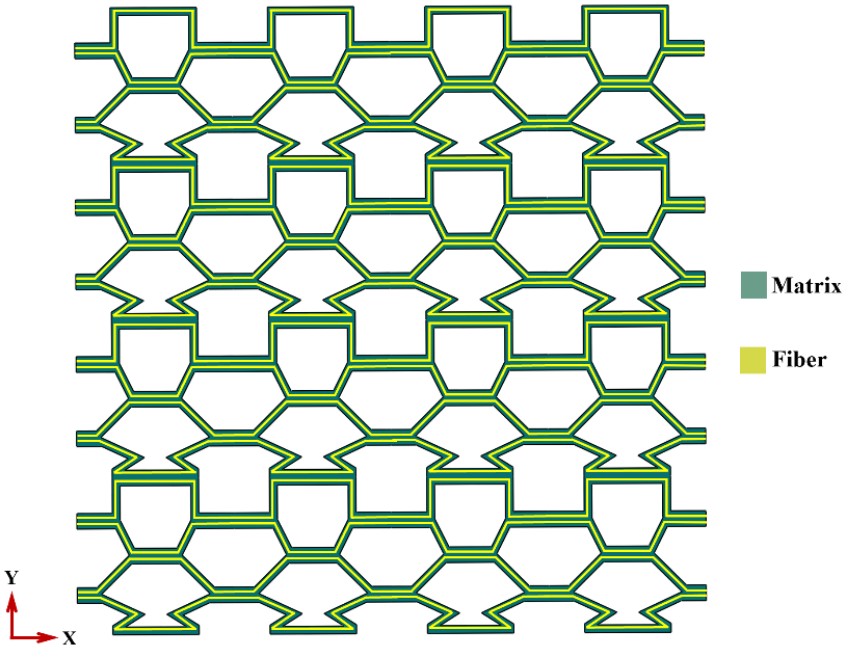

(a)

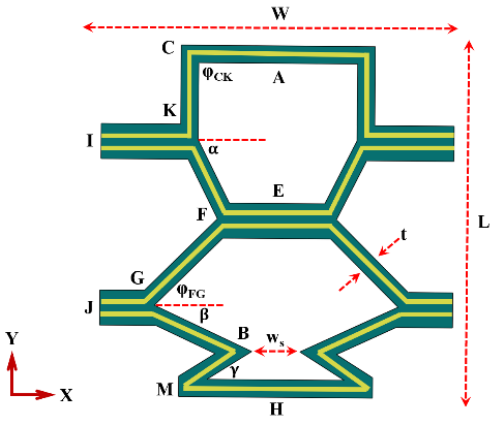

(b)

Figure 3. Configuration of the composite bone-inspired unit cell in tessellation (a), geometrical parameters of the composite bone-inspired unit cell (b).

Table 1. Geometrical parameters of bone-inspired unit cell.

CA	5mm	FE	2.76mm	BM	3.8mm	φ_{FG}	45°
CK	5mm	FG	7.07mm	MH	5.61mm	α	63.43°
KI	5mm	GJ	2.24mm	t	1mm	β	25°
KF	5mm	GB	5.92mm	φ_{CK}	90°	γ	41.14°

3.Design Optimization

3.1. Developed analytical model

Castigliano's second theorem was used to calculate the elastic properties of the bone-inspired unit cell in the y-direction. The structure, introduced as baseline structure, was loaded under y-direction using FEA. Deformation of the unit cell was observed, and the boundary conditions were extracted. Due to symmetry, half of the unit cell was considered, and the free diagram of the unit cell is shown in Fig.4.

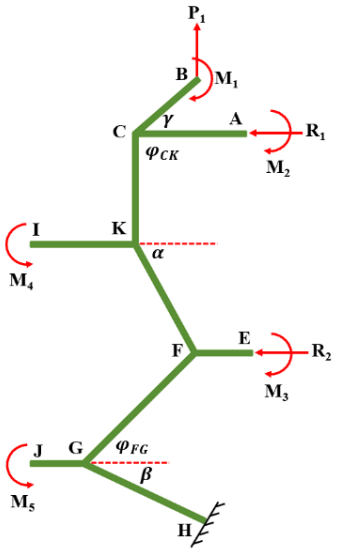

Figure 4. Free diagram of half of the unit cell under loading y-direction

R_1 and R_2 are considered reaction loads, P_1 is the force acting in the y-direction, and M_1, M_2,

M_3, M_4, and M_5 represent the reaction moments at points B, A, E, I, and J, respectively. Internal forces and moments are obtained by writing the equilibrium equation in every strut of the unit cell, which the details of the equations are represented in [42]. The strain energy of an isotropic ply under a combination of axial and bending loads is obtained as Eq.1.

$$U_{axial} = \frac{1}{2}\left(\int_0^l \left(\frac{F^2}{AE}dx + \frac{M^2}{EI}dx\right)\right) \quad (1)$$

An orthotropic ply (Fig.5) with unidirectional fibres in the x-direction is considered for developing an analytical model.

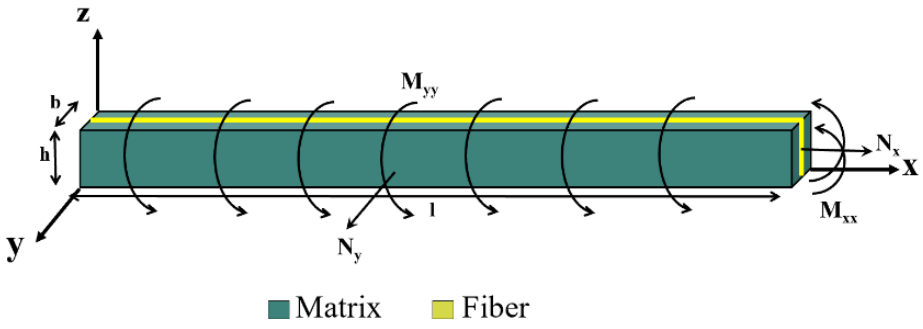

Figure 5. Forces and moments resultants in an orthotropic ply

The classical laminated theory (CLT) was employed to expand isotropic equations to orthotropic. According to this theory assumptions, thickness shear strains (γ_{xz}, γ_{yz}) and the out-of-plane stress (σ_{zz}) are zero. The strain distribution in orthotropic ply is considered as Eqs.2a and 2b.

$$\varepsilon_{xx} = \varepsilon^0_{xx} + z\kappa^0_{xx} \quad (2a)$$

$$\varepsilon_{yy} = \varepsilon^0_{yy} + z\kappa^0_{yy} \quad (2b)$$

The total strain energy of the ply it can be drive as Eq.3.

$$U_{axial} = \frac{1}{2}\int_V (\sigma_{xx}\varepsilon_{xx} + \sigma_{yy}\varepsilon_{yy})\, dV \tag{3}$$

Forces and moments resultants in Fig.5 are written as Eqs.4a-4d.

$$N_x = \int_{-\frac{h}{2}}^{\frac{h}{2}} \sigma_{xx}\, dz \tag{4a}$$

$$N_y = \int_{-\frac{h}{2}}^{\frac{h}{2}} \sigma_{yy}\, dz \tag{4b}$$

$$M_{xx} = \int_{-\frac{h}{2}}^{\frac{h}{2}} \sigma_{xx} z dz \tag{4c}$$

$$M_{yy} = \int_{-\frac{h}{2}}^{\frac{h}{2}} \sigma_{yy} z dz \tag{4d}$$

In the axial loading condition, the curvature of the reference surface is zero, so axial strain energy can be calculated as Eq.5.

$$U_{axial} = \frac{1}{2}\int_V (\sigma_{xx}\varepsilon^0_{xx} + \sigma_{yy}\varepsilon^0_{yy}) dV = \frac{1}{2}\int_0^l \int_0^b (N_x\, \varepsilon^0_{xx} + N_y \varepsilon^0_{yy}) dx dy \tag{5}$$

Where The force resultants are defined as $N_x = \frac{F_x}{b}$ and $N_y = \frac{F_y}{l}$. Also, Moment resultants in Fig.5 are defined as $M_x = \frac{M_{xx}}{b}$ and $M_y = \frac{M_{yy}}{l}$. The midplane strain components are zero in the bending moment, so bending strain energy can be calculated as Eq.6.

$$U_{bending} = \frac{1}{2}\int_V (\sigma_{xx}(z\kappa_{xx}^0) + \sigma_{yy}(z\kappa_{yy}^0))dV = \frac{1}{2}(\int_0^l \frac{M_{xx}^2}{E_{11}I_{yy}}dx + \int_0^b \frac{M_{yy}^2}{E_{22}I_{xx}}dy) \quad (6)$$

As a result, for an orthotropic ply, the total strain energy in a global coordinate system can be derived as Eq.7.

$$U_{tot} = \frac{1}{2}(\int_0^l \frac{F_x^2 l}{A_x E_{11}}dx + \int_0^b \frac{F_y^2 b}{A_y E_{22}}dy + \int_0^l \frac{M_{xx}^2}{E_{11}I_{yy}}dx + \int_0^b \frac{M_{yy}^2}{E_{22}I_{xx}}dy) \quad (7)$$

Where $A_x = b \times h$ and $A_y = l \times h$ are the cross section of the ply normal to the x and y axes. The displacement δ_y is obtained using the total strain energy and Castigliano's second theorem at P_1. Then, by calculating stress and strain, Hooke's law obtains the elastic modulus. The total relation of the young's modulus is presented in Eq.8 and the extended equation is presented in [42].

$$E_y = F(E_s, E_{11}, L, \mathrm{l}, W, D, t, \beta) \quad (8)$$

It is worth noting that while the located fibres in diagonal struts are not capable of transforming the applied compressive loading, the mechanical properties of the pure PLA are assigned for these struts.

3.2. Optimization algorithm

Particle Swarm Optimization (PSO) is a heuristic global optimization method based on swarm intelligence [43] . In this algorithm for a randomly initialized set of solutions in the solution space, particles update themselves by following two optimal positions (P_{best}, G_{best}) in each iteration. The best experience position searched by the particles is named the individual optimal position P_{best}, while the current optimal position searched by all particles is recorded as the optimal global position G_{best}. For the D-dimensional vector in particle i, the positions and

velocities can be expressed as $x_i = (x_{i1}, x_{i2}, \dots , x_{iD})$ and $v_i = (v_{i1}, v_{i2}, \dots , v_{iD})$, respectively. The updating formulas can be defined as Eqs.9 and 10.

$$v_{ij}(k+1) = \omega \,.\, v_{ij}(k) + c_1 r_1 \left(P_{best\,ij}(k) - x_{ij}(k)\right) + c_2 r_2 \left(G_{best\,j}(k) - x_{ij}(k)\right) \quad (9)$$

$$x_{ij}(k+1) = x_{ij}(k) + v_{ij}(k+1),\ j = 1, 2, \dots, D \quad (10)$$

$P_{best\,i} = (P_{best\,i1}, P_{best\,i2}, \dots, P_{best\,iD})$ is the best position for the i-th particle that has ever been experienced and $G_{best} = (G_{best\,1}, G_{best\,2}, \dots, G_{best\,D})$ is the best position that all the particles have ever experienced. Two independent random functions r_1 and r_2 are in the range of (0, 1).

In this study, a PSO algorithm was employed to obtain maximum and optimum elastic modulus due to Eq.8 which is presented in the above section. The main parameters of the PSO algorithm are ω, c_1, c_2, number of population, and iterations. The range of these parameters is selected based on reported data in [44] and was obtained by trial and error in this study. The best parameters for this subject are presented in Table 2.

Table 2. Parameters of PSO algorithm

Parameters	values
Number of populations	50
Number of iterations	100
c_1 and c_2	2
ω	1

Also, some constraints were defined in the algorithm to obtained optimum cellular structures. Important geometrical parameters in the bone-inspired unit cell are defined as α, β, γ, CA, FE.

The related constraints are included: 40°< α <90°, 15° < β <130°, 30°< γ <90°, 3< CA <6, 1< FE <6 and dimensions of the structures must be 20mm×20mm×20mm. The objective function is considered as calculation of the elastic modulus of the unit cell. The procedure of the PSO algorithm in this study is shown in Fig.6. Fig.7 illustrates the best fitness per iteration, and demonstrates that the objective function has converged to its maximum value.

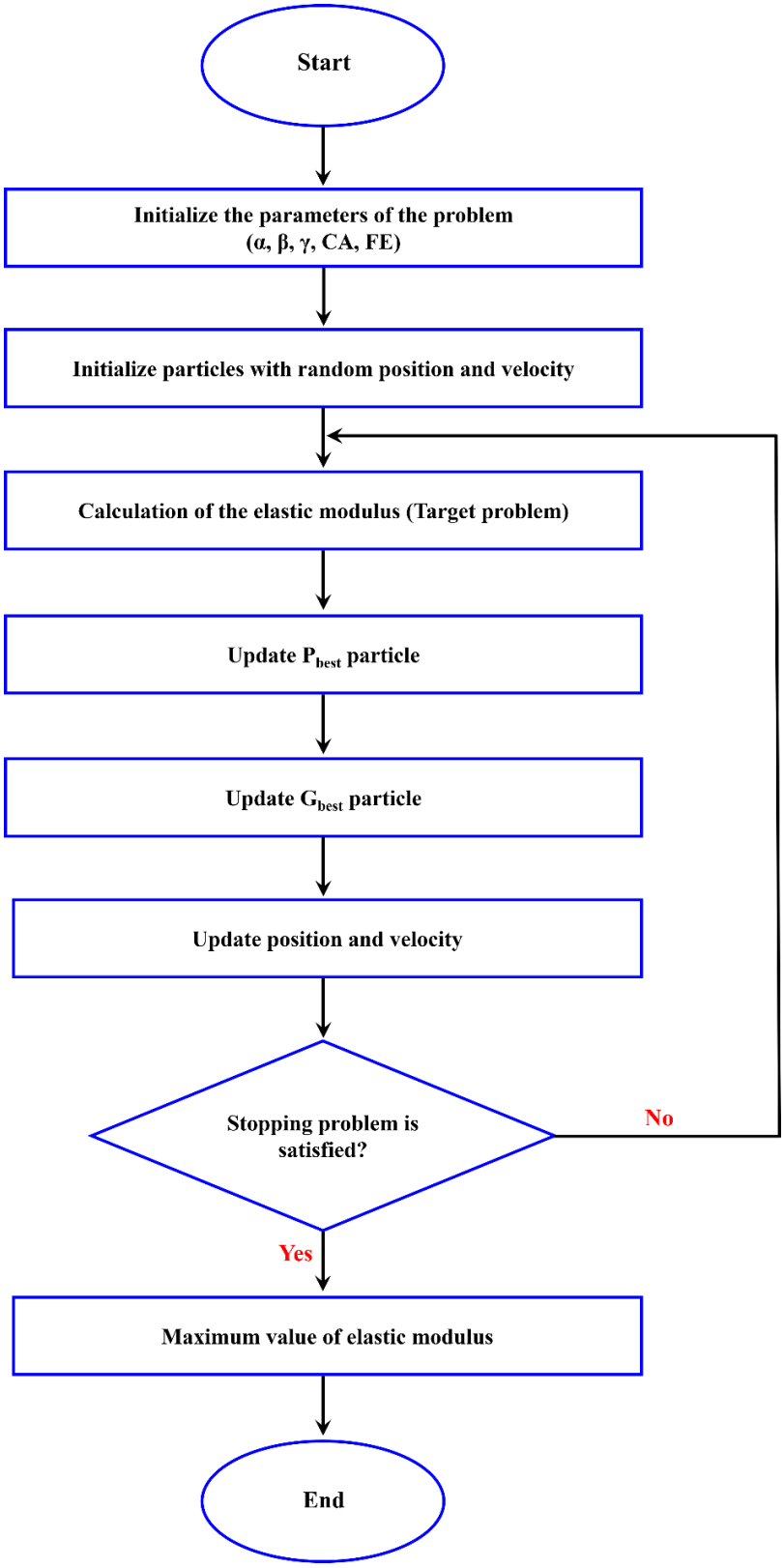

Figure 6. Optimization procedure to obtained cellular structures geometry

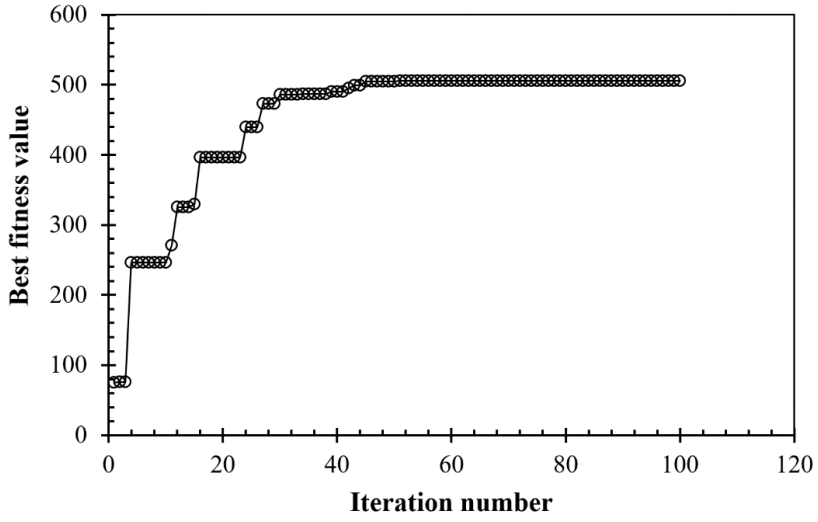

Figure 7. Best fitness per iteration

The final configuration reported by optimization showed in Fig.8a. This structure has the maximum young's modulus that PSO obtained. As this figure shows, some struts are approximately vertical, and it can cause buckling during compression loading. So, the optimum structure is introduced as the highest stiffness structure, which prevents buckling (Fig.8b). This response is obtained by evaluating buckling in several PSO responses by FEA. The geometric parameters of these structures are presented in Table 3a and 3b. The optimized cellular structures will be considered in numerical simulations to assess the effect of stiffness on the energy absorption capacity.

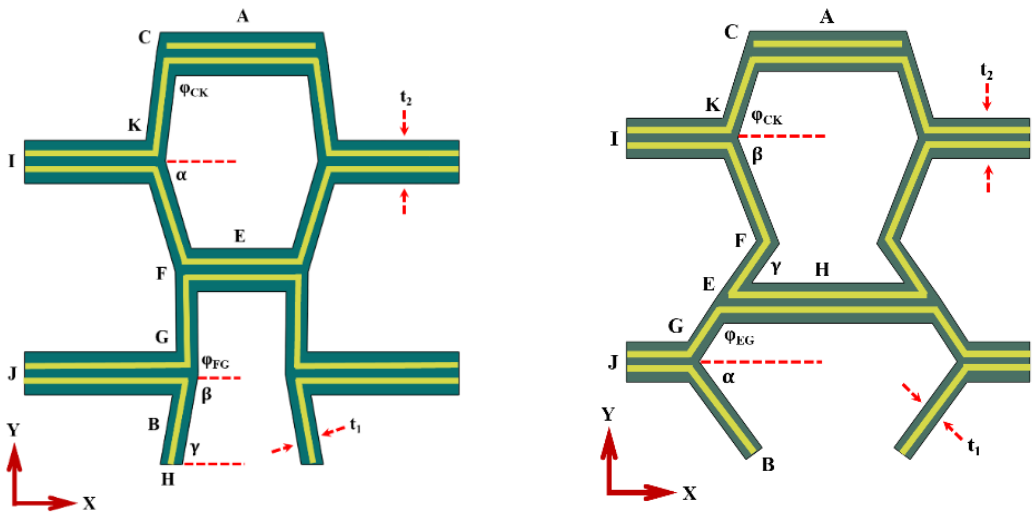

Figure 8. Maximum stiffness unit cell (a), optimum stiffness unit cell (b).

Table 3. Geometrical parameters of optimized unit cells.

(a) Maximum stiffness unit cell							
CA	3.42mm	FE	2.55mm	BH	1.01mm	φ_{FG}	98.09°
CK	5.03mm	FG	4.78mm	t_1	1mm	α	73.59°
KI	5.97mm	GJ	7.49mm	t_2	2mm	β	100°
KF	5.12mm	GB	4.28mm	φ_{CK}	96.9°	γ	100°
(b) Optimum stiffness unit cell							
CA	3.66mm	FE	3.69mm	GB	5.64mm	φ_{EG}	122.91°
CK	4.53mm	EH	5.1mm	t_1	1mm	α	53.79°
KI	5mm	FG	3.48mm	t_2	2mm	β	68.62°
KF	5.55mm	GJ	3mm	φ_{CK}	72.85°	γ	54.76°

4. Experimental Methods

4.1. Material and 3D printing method

Polylactic acid (PLA) filament was utilized to produce the bio-inspired cellular structure, as mentioned in Fig.9a. The specimen was made with 80mm×80mm×20mm dimensions. The proposed structure was reinforced with continuous E-glass fiber and fabricated with a Fused Filament Fabrication (FFF), as shown in Fig.9a. According to [45], a special nozzle has been designed to prepare all composite samples with continuous fiber for the simultaneous impregnation system. A nozzle diameter of 0.5 mm and the outer nozzle diameter of 1 mm were employed, and the inlet on the side surface of the nozzle was considered. Also, fiber with a diameter of 0.1 mm was used. The process of fabricating and printing is shown in Fig.9b. According to this figure, the glass fiber enters the melting chamber through its inlet on the side surface of the nozzle, and the impregnated fibres are guided out of the nozzle and placed on the building plate. The reinforced sample's printing speed is 10 mm/s, and the nozzle temperature and the printing bed are set to 200 and 60℃, respectively.

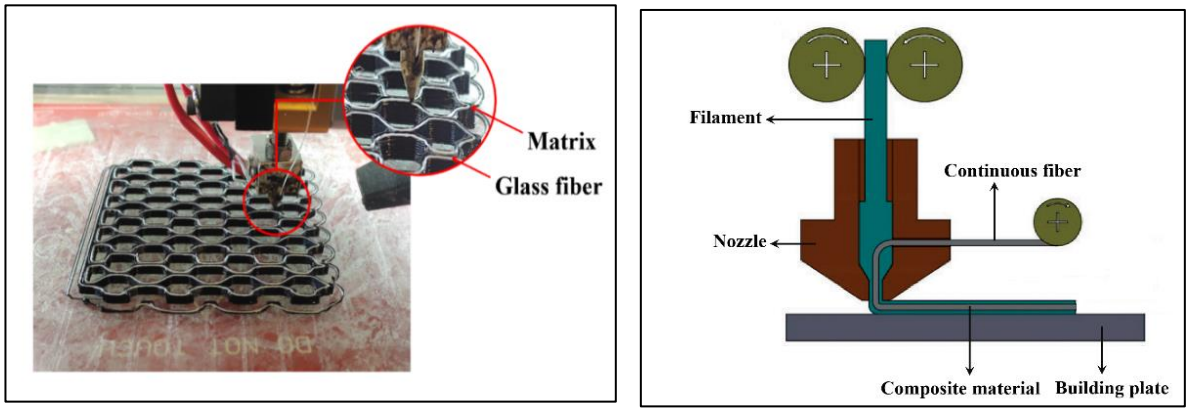

(a) **(b)**

Figure 9. (a) Printing process of bone-inspired cellular structure, (b) Mechanism of FFF 3D printing with continues fiber [45].

4.2. Tensile test for raw material

ASTM-D638 was used to obtain the mechanical properties of PLA. The specimen was designed in CATIA software and manufactured with the FFF 3D printer (Fig.10). The PLA used for this study was provided by Z.F. filaments private limited company. Three specimens were manufactured and subjected to a tensile test at a 5 mm/min speed by the Instron 5500R test machine. Table 4 represents the mechanical properties of pure PLA material under the tensile test.

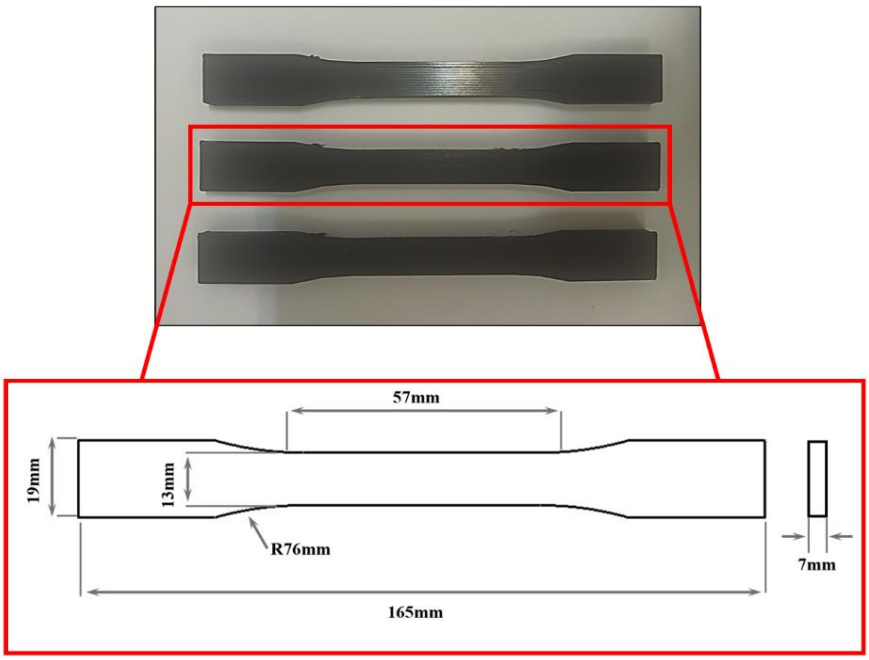

Figure 10. 3D printed tensile test specimens based on ASTM-D638 standard

Table 4. Mechanical properties of Polylactic acid (PLA) material

Type	Young's modulus (GPa)	Poisson's ratio	Yield stress (MPa)	Ultimate Tensile Strength (MPa)	Fracture Strain
PLA	3.3	0.35	22.76	58.29	0.01025

4.3. Uniaxial compression test for the cellular structure

Composite cellular structures were subjected to the compression test in the y-direction (Fig.11). A minimum of two samples were tested for these studies. A SANTAM test machine was utilized to perform compression tests. A cross-head speed of 5 mm/min was selected for the test condition. Force-displacement data was obtained from the test machine to study the energy absorption capability of the cellular structure in the y-direction. A high-speed camera was employed to investigate the deformation and failure mechanisms in samples (Fig.12).

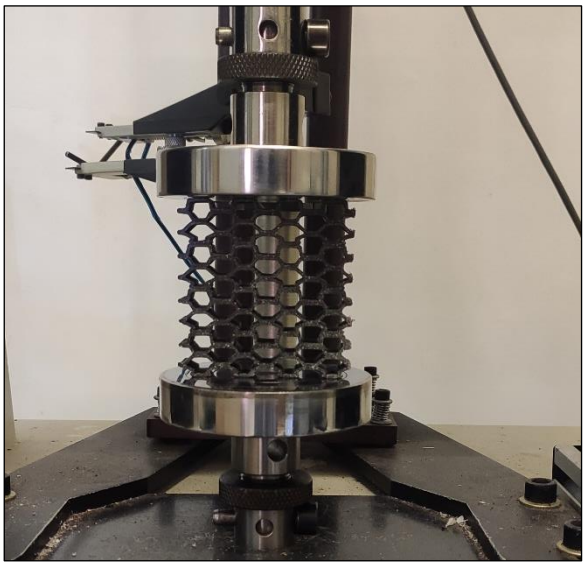

Figure 11. Compression test under loading in the y-direction

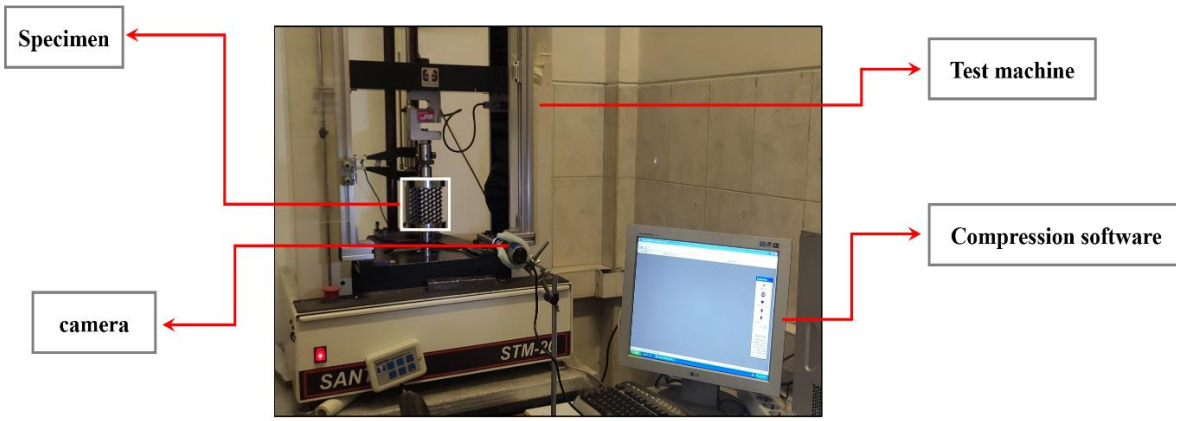

Figure 12. Experimental test of specimen under compression test

5. Numerical simulation

Finite element analysis (FEA) was used to assess the energy absorption capacity in bone-inspired and optimized cellular structures. An ABAQUS explicit solver (version 2018) was used for simulation. A 3D stress finite element model was simulated and the C3D8R element was utilized to mesh the model. The cellular structure was placed between two rigid plates to simulate a compression test, and uniaxial force in the y-direction was applied. The rigid top plate can only move in the y-direction, and the rigid bottom plate was completely fixed. Boundary conditions considered for simulations are shown in Fig.13.

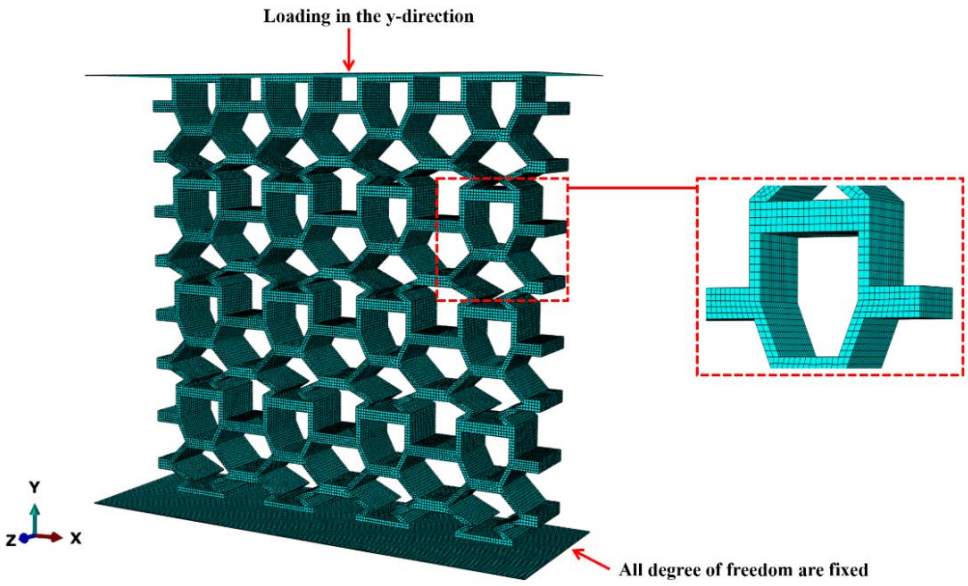

Figure 13. Boundary condition applied in numerical simulation under loading in the y-direction.

A displacement control condition was utilized for simulations. Contact behaviour was defined as tangential with a coefficient of friction equal to 0.2 for all surfaces [33]. Also, the general contact is applied to the cellular composite structure to model the contact behaviour. A mesh convergence analysis was also implemented, and a mesh size of 0.5 mm was chosen based on a convergence of elastic modulus in each simulation.

VUSDFLD subroutine was employed to assign the material behaviour of a composite bone-inspired structure. Due to damage growth, several field variables were defined to simulate mechanical property decreases in composite cellular structure. The struts of the unit cell were modelled as an orthotropic material, and equivalent mechanical properties of fiber-reinforced PLA were assigned. Ultimate tensile stress of the PLA and Fiber-reinforced PLA was chosen as 60 MPa and 157 MPa, respectively. Fig.14 shows the procedure for conducting FEM. Maximum stress criteria were used to assess decreasing mechanical properties of the fiber-reinforced bio-inspired structure. According to the assumption in this criterion, shear stress isn't considered.

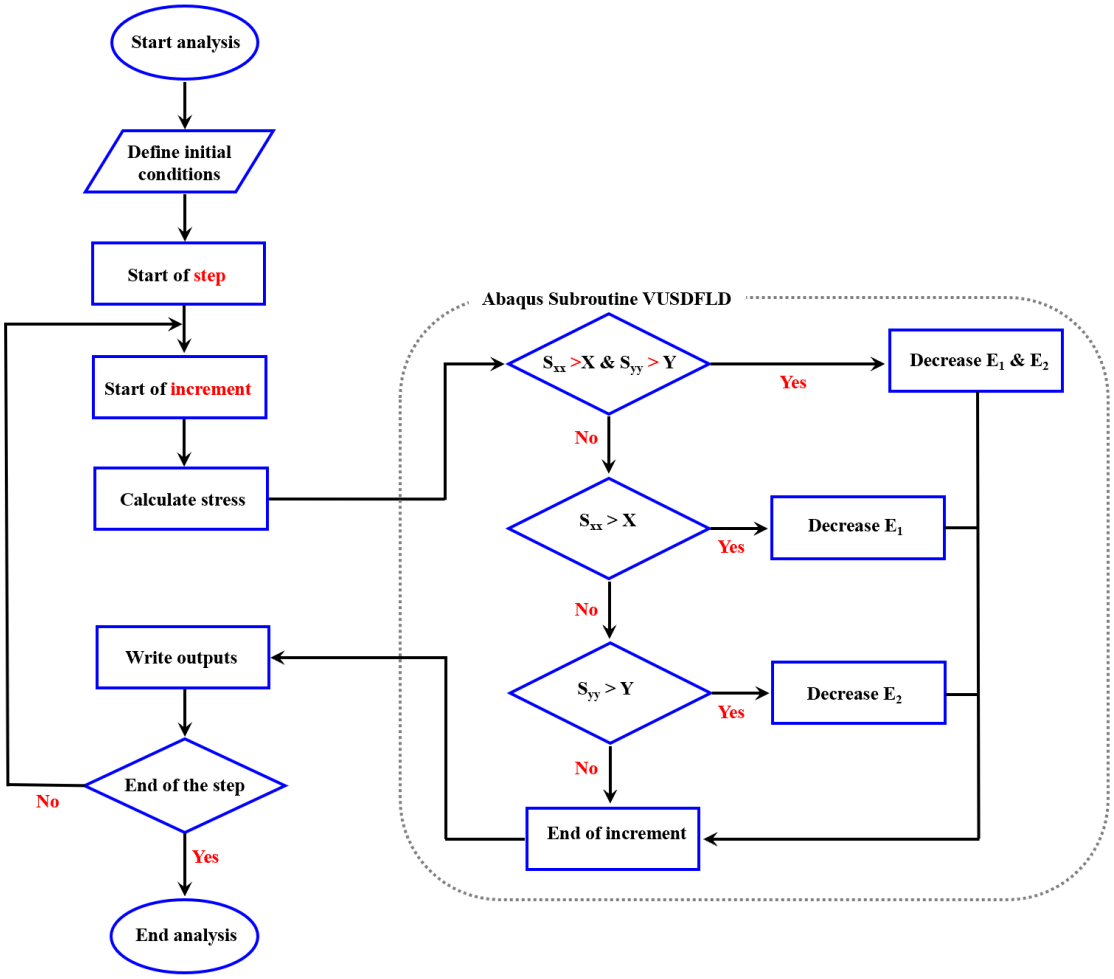

Figure 14. A procedure of the VUSDFLD subroutine in FEM.

This figure defines X and Y as ultimate tensile stress in the x and y directions. According to

this algorithm, if the S_{xx} (stress in the fiber direction) > 157 MPa and S_{yy} (stress in the perpendicular direction of the fiber) > 60 MPa at the same time, the E_1 and E_2 decrease, so the fiber and matrix failure are accrued. In other states, if the S_{xx} > 157 MPa and S_{yy} < 60 MPa, only E_1 decreases, and fiber failure is accrued. In the final state, if the S_{yy} > 60 MPa and S_{xx} < 157 MPa, only E_2 is decreased, so matrix failure is accrued.

Mechanical properties of fiber-reinforced-PLA have been obtained in a previous study in the Tarbiat Modares fracture mechanics laboratory [33]. Due to the different filament brand was used, the rule of mixture equation was used to get the E_c according to Eq.11.

$$E_c = E_{11} = E_m(1 - V_f) + E_f V_f \tag{11}$$

Where E_m is considered 3.3 GPa, E_f and V_f is obtained based on a previous study in [33]. The fiber volume fraction is obtained at 23% by getting the E_c. Mechanical properties considered in the numerical simulation are presented in Table 5.

Table 5. Mechanical properties of fiber-reinforced-PLA.

Type	E_1 (GPa)	E_3 E_2 & (GPa)	G_{12}, G_{13} & G_{23} (GPa)*	ν_{12}, ν_{13} & ν_{23}*
Fiber-reinforced-PLA	9.574	3.3	0.8	0.18

*These parameters are assumed.

6. Results and discussion

6.1. Energy absorption of a bone-inspired structure

Compression tests were conducted to investigate Energy Absorption (EA) in a composite bone inspired cellular structure in the y-direction (Fig.11 and 12). Force-displacement data under

loading in the y-direction is shown in Fig.15. EA capacity in different displacements was also shown in this figure.

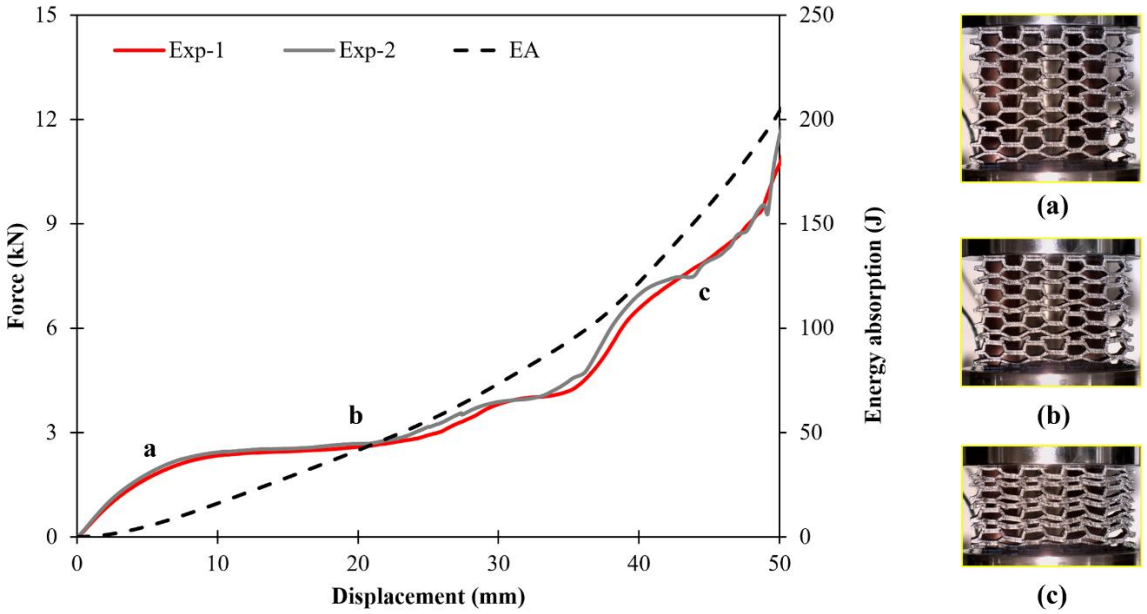

Figure 15. Force-displacement of bone-inspired structure in the y-direction.

A minimum of two specimens were utilized to conduct the experimental test. There is a linear elastic region at the start of the compression loading in which the force reaches to its initial peak at 2kN. In this region, the first damage in the composite cellular structure occurs, as shown in Fig.15a. The elastic-plastic transition region appears after the initial peak force. After this region, the cellular structure has plastic deformation. Continuing the compressive loading, the plateau stress region obtained in this region indicates that the structure has a uniform deformation, and the force is distributed almost uniformly. This region is shown in Fig.15b. All straight struts have double thicknesses in comparison with diagonal struts. With continuing the loading, diagonal struts are placed on top of one another, and, consequently, the structure's stiffness and force increase. After collapsing the structure and destroying all the rows at the end of the experimental testing, the structure has become denser, and the force value has increased upwards. Deformation of the structure in this area is shown in Fig.15c. EA diagram shows that the amount of energy absorption increases with collapsing the structure and rising

the displacement.

Matrix and fiber failures of the bone-inspired composite structure in the collapsing condition are shown in Fig.16.

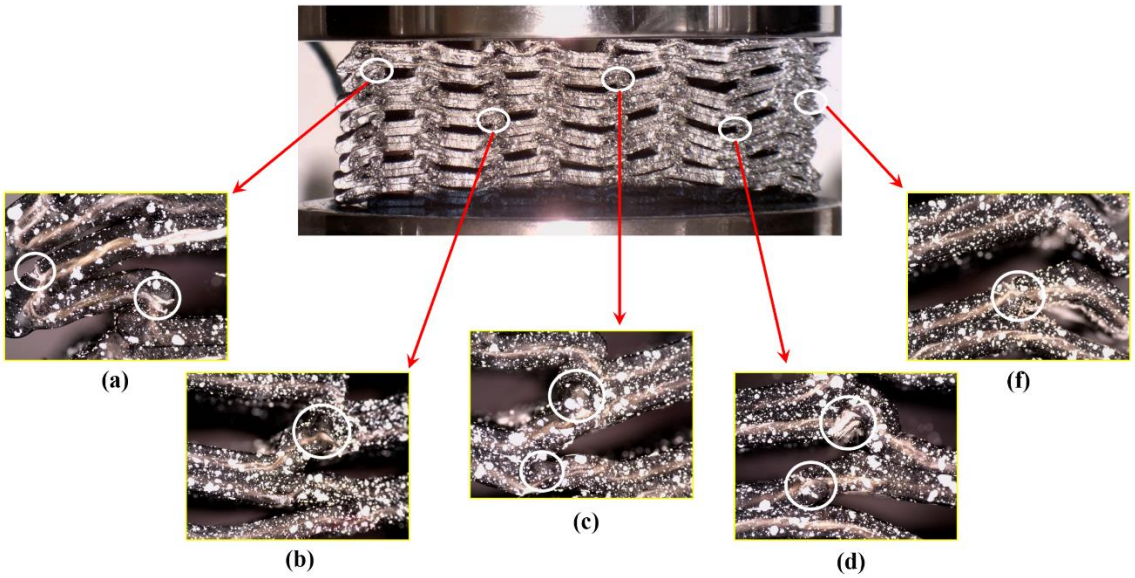

Figure 16. Cracks and failures in the composite cellular structure

According to Fig.16a, some areas in the structure are subjected to matrix failure and cracks which causes the failure of the fibres. Also, some areas are undergoing plastic deformations which are shown in Figs.16b and 16c with white circles. Fig.16d shows the extrusion of fiber from the matrix and a small crack which is caused matrix failure in the structure, this situation is also seen in Fig.16f.

The Specific Energy Absorption capability and Crush Load Efficiency are calculated to investigate the energy absorption properties in a bone-inspired cellular structure. These parameters are critical key parameters for comparing the performance of cellular structures. Specific Energy Absorption and Crush Load Efficiency are calculated using Eqs.12 and 13. Specific Energy Absorption is obtained by calculating total energy absorption divided by mass, and Crush Load Efficiency is also calculated by mean crushing load divided to initial peak

force.

$$SEA = \frac{Total\ energy\ absorption\ (EA)}{Total\ specimen\ mass} = \frac{\int Fdx}{m} \tag{12}$$

$$CLE = \frac{Mean\ Crushing\ Load}{Initial\ Peak\ Crushing\ Force} = \frac{MCL}{IPCF} \tag{13}$$

MCL parameter in Eq.13 is obtained by Eq.14. This parameter is calculated by total energy absorption divided by maximum crushing displacement. The maximum crushing displacement is selected based on the beginning of the densification area in the force-displacement diagram.

$$MCL = \frac{Total\ Absorbed\ Energy}{Maximum\ Crashing\ Displacement} = \frac{\int Fdx}{d_{max}} \tag{14}$$

Table 6 represents the energy absorption parameters in the bone-inspired unit cell under loading y-direction.

Table 6. Energy absorption parameters in the composite bone-inspired cellular structure (CBIS).

Specimen	Mass (gr)	EA (J)	SEA (J/kg)	CLE	d_{max} (mm)	IPCF (kN)	MCL (J/mm)
CBIS	49	96.82	1976.07	1.38	35	2	2.76

6.2. FEM of energy absorption analysis

6.2.1. Energy absorption capacity in a bone-inspired structure

Fig.17 shows the FEM and experimental force-displacement data under compressive loading

in the composite bone-inspired cellular structure. The deformation mechanism in different displacements is also shown in this figure. The experimental and numerical results are in a very good agreement. In the first area of the diagrams, the linear elastic region is seen, which is predicted well by the numerical model. The deformation of the structure in this area is presented in Fig.17 at the displacement of 4mm for numerical and experimental results. The structure has nonlinear behaviour with continuous loading and after the initial peak force at 2kN. The plateau stress region appears by continuing the loading. The structure has a uniform deformation in this area that the force is distributed almost uniformly throughout the structure. According to the force-displacement diagram related to the numerical method, the plateau stress region shows a good agreement with the experimental curve. Deformation of the structure in this region showed in Fig.17 for numerical and experimental results at a displacement of 14mm. Some examples of deformed struts in the cellular structure are noted in this figure by circles to compare numerical and experimental results. It can be seen that the numerical model predicts a similar deformation behaviour in the bio-inspired structure for the struts. By collapsing the structure, the diagonal struts are placed on top of one another other that increases the stiffness of the structure. Therefore, the amount of force continuously rises. Images of collapsed specimens from experimental and numerical results at the displacement of 24mm support this discussion. With continuous compressive loading, the structure collapses completely, and a densification area emerges in the force-displacement curve. Experimental and numerical deformation in Fig.17 (u=34 mm) is related to this region. For this stage, differences between numerical and experimental are evident. This is due to manufacturing tolerances producing specimens that are not perfectly symmetric, while in modelling the geometry of specimens are considered to have perfect size and alignment.

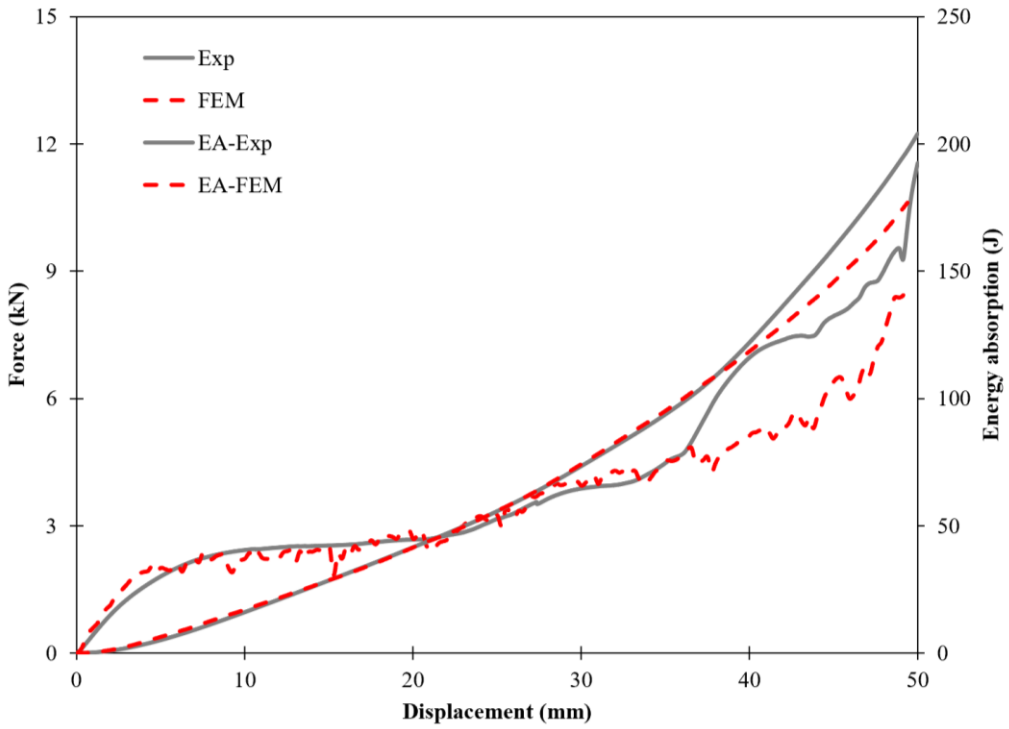

Numerical	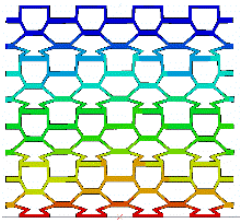	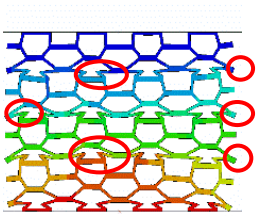	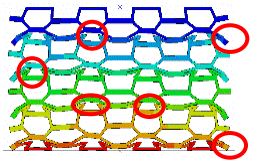	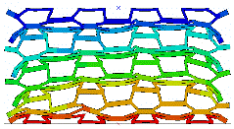
Experimental	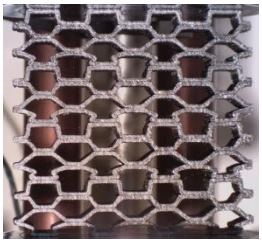	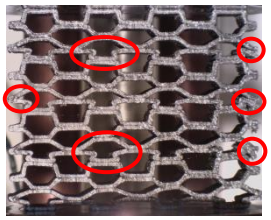	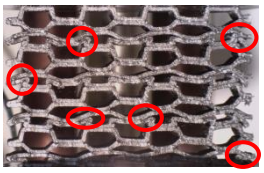	
u (mm)	**4**	**14**	**24**	**34**

Figure 17. Comparing the experimental test and numerical analysis of the bone-inspired structure under loading in the y-direction.

EA diagrams are shown in Fig.17. It is demonstrated that raising the displacement and collapsing the cellular structure increases the amount of energy absorption. Fig.18 shows the EA and SEA in the composite bone-inspired unit cell experimentally and numerically at the displacement of 35 mm. For EA and SEA values, the differences between the experimental and numerical results are reasonable. In general, the numerical simulation model has enough

accuracy in predicting the mechanical behaviour and deformation mechanism in the composite bone-inspired cellular structure.

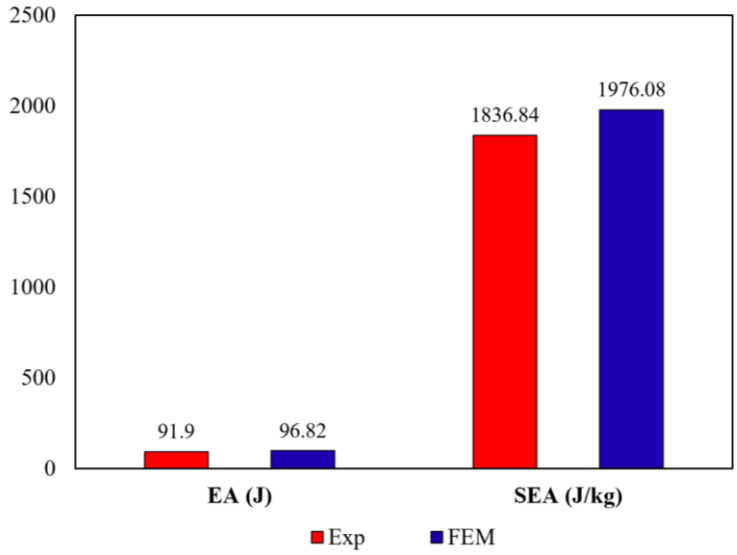

Figure 18. EA and SEA in the composite bone-inspired cellular structure.

6.2.2. Effect of fiber reinforcement on energy absorption capability

FEM was employed to assess the energy absorption capability of bio-inspired cellular structures for two materials: a pure PLA and a PLA reinforced with glass fibres. Boundary conditions mentioned in section 5 were used for each FEM simulation. Fig.19 shows the force-displacement curves for loading in the y-direction.

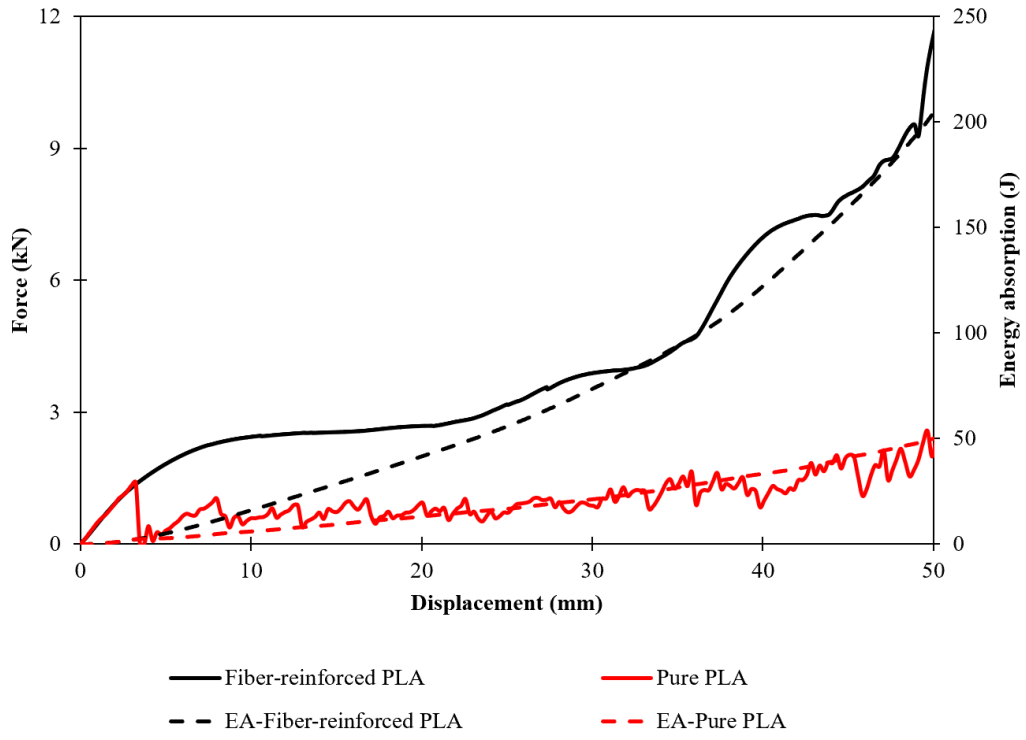

Figure 19. Force-displacement curve of Pure PLA and Fiber-reinforced PLA cellular structure under loading in the y-direction.

In the initial region of the force-displacement curve in the pure PLA structure, the first damage occurred after reaching the peak force of 1.4 kN. Subsequently, the force suddenly decreased and reached to zero. Continuing the loading, for the pure PLA cellular structure, some upwards and downwards appeared in the force-displacement diagram which are due to formations of local catastrophic damages in different parts of the cellular structure. In the force-displacement curve of the cellular structure, the fiber-reinforced PLA cellular structure (composite PLA cellular structure) showed higher mechanical performance compared to the pure PLA structure. The composite cellular structure appears useful for energy absorption applications due to preventing catastrophic local failure that results in a smoother behaviour compared to the pure PLA structure. By comparing these diagrams for the pure and composite PLA cellular structures, it was evident that the gradient of the force-displacement curve (stiffness) in fiber-reinforced structure and the amount of peak force was significantly higher than in the pure PLA structure. Also, the fiber-reinforced cellular structure diagram has a more usable plateau stress

region than the pure PLA structure due to adding fibres and continuous deformation. In both diagrams, EA capability increased with rising the displacement and collapsing the structure. In the fiber-reinforced cellular structure, the EA capability is significantly higher compared to the pure PLA structure at the same displacement. The amount of EA and SEA in the composite bone-inspired structure and un-reinforced cellular structure is shown in Fig.20. It should be noted that, the displacement of 35 mm is considered for calculating these parameters. As shown in Fig.20 EA and SEA capabilities in fiber-reinforced cellular structure improved by 254% and 225% compared to the pure PLA structure, respectively. As a result, it can be found that mechanical performances are increased by utilizing fiber in the cellular structures.

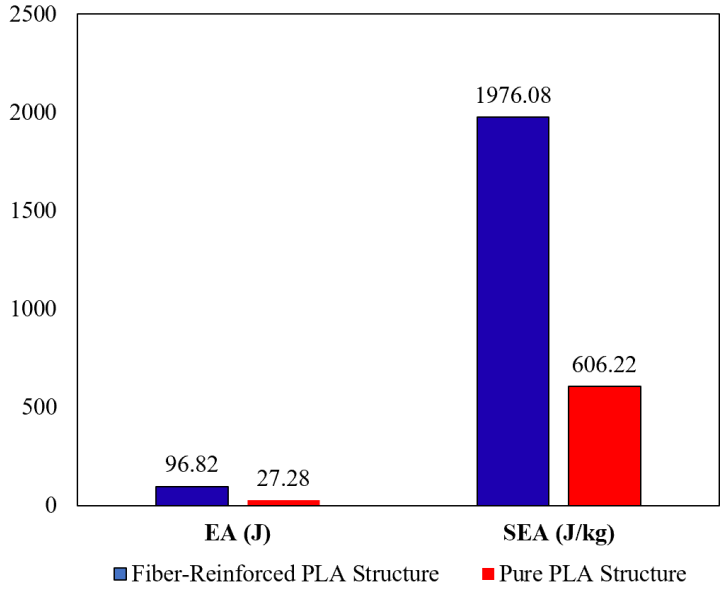

Figure 20. EA and SEA in the fiber-reinforced and pure PLA cellular structure.

6.2.3. Effect of unit cell designs on energy absorption

This section investigates the effect of unit cell's geometrical parameters on the energy absorption capability of cellular structure. As discussed in section 3.2, a PSO optimization algorithm was used to design two different unit cells for the bio-inspired cellular structures to obtain the maximum and optimum stiffnesses in the cellular structures compared to a baseline

unit cell. These unit cells were designed to assess the effect of stiffness on the energy absorption capability. Force-displacement diagrams for each cellular structure are represented in Fig.21.

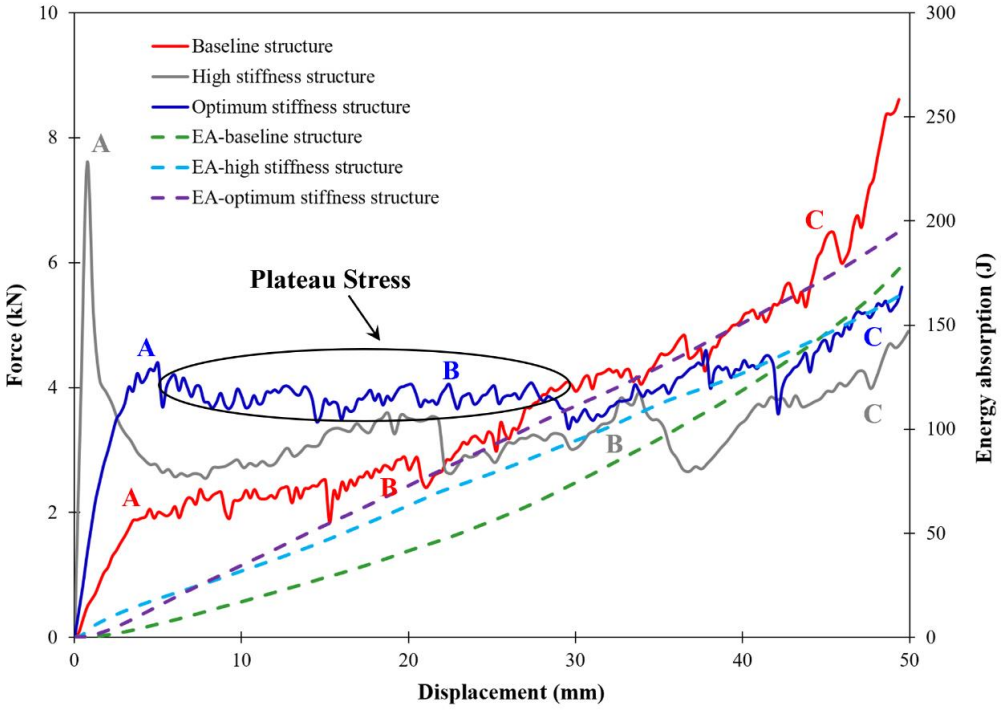

Figure 21. FEM force-displacement diagrams in baseline and optimized cellular structures.

The deformation behaviours of the cellular structures at different points of diagrams are also shown in Fig.22. For the baseline structure, the initial peak force was 2kN. Subsequently, a plastic deformation occurred in the structure in which the diagonal struts were placed on top of each other that increased the stiffness of the structure. Therefore, the amount of force continuously increased and reached to the densification region (Fig. 22c). For the structure with maximum stiffness, the initial peak force was 8 kN (Point A). After the initial peak force, the amount of force suddenly dropped to 3 kN. In this region, the buckling occurred in the structure (Fig. 22d). By continuing compressive loading, the structure collapsed (Figs. 22e and f). For the structure with optimum stiffness, the peak force was 4.5 kN (A). After the peak force, a large plateau stress region is evident. In this region, the structure experiences a uniform force and does not face a sudden and severe rise and fall of the force. By further deformation, the

structure collapsed (Fig. 22i).

Points in the diagram	**A**	**B**	**C**
Baseline structure	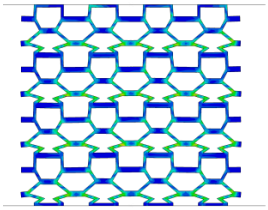	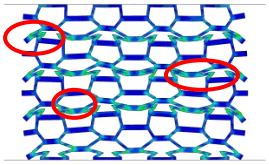	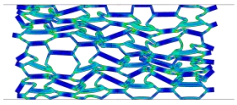
	(a)	**(b)**	**(c)**
Maximum stiffness structure	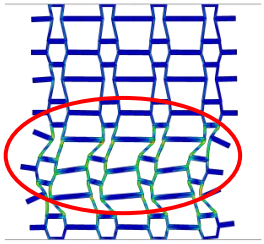	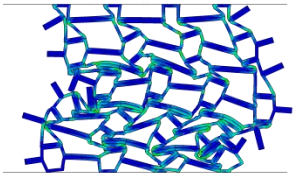	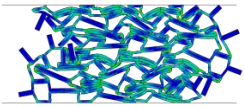
	(d)	**(e)**	**(f)**
Optimum stiffness structure	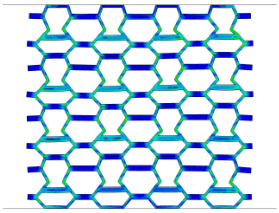	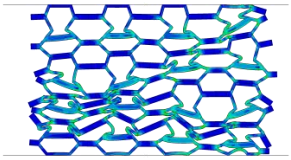	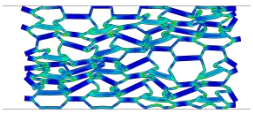
	(g)	**(h)**	**(i)**

Figure 22. FEM deformations in baseline and optimized cellular structures

By comparing the force displacement diagrams for the cellular structures, it is clear that by changing the geometrical parameters in the unit cells of the structures, the stiffness (the gradient

of curves) can be tailored to design a cellular structure with an optimized stiffness for energy absorption applications. Furthermore, the amount of initial peak force significantly increases by increasing the stiffness of the structures based on the geometrical parameters of the unit cells. The structure with the optimum stiffness exhibits a large stable plateau stress region. Also, Fig.21 shows the force-displacement and energy absorption diagrams for the baseline cellular structure compared to cellular structures with maximum and optimized stiffnesses. According to this figure, the amount of energy absorption capacity increased by collapsing the structures, and the optimized cellular structures show higher energy absorption than the baseline cellular structure. Therefore, this design can be used to increase the energy absorption capacity with high potential to be used in energy absorption applications. The EA parameters for the baseline, maximum stiffness and optimized cellular structures are summarized in Table 7. Compared to the baseline structure, the EA capability in maximum stiffness and optimum stiffness structures are improved by 63% and 60%, respectively. Also, the SEA value increased in maximum stiffness and optimum stiffness structures by 66% and 67%, respectively. CLE is another important parameter in the energy absorption capability. The structures with a CLE value of 1 have ideal properties for applications in energy absorption [46]. Based on the CLE value of the structures, the optimum stiffness structure is closer to 1 and has higher SEA than other cellular structures. So, it can be a useful cellular structure in energy absorption applications.

Table 7. Energy absorption parameters in Baseline and optimized structures.

Specimen	Mass (gr)	EA (J)	SEA (J/kg)	CLE	d_{max} (mm)	IPCF (kN)	MCL (J/mm)

Baseline	49	96.82	1976.07	1.38	35	2	2.76
Maximum stiffness	48	158.20	3295.88	0.43	47.68	7.60	3.31
Optimum stiffness	47	155.85	3315.97	0.84	41.88	4.38	3.72

Conclusion

The main of this investigation was to analysed the mechanical response of additively manufactured composite bone-inspired cellular structures and assess the effect of topology optimization on the energy absorption capability. In this regard, samples were manufactured additively from fiber-reinforced PLA with the use of a FFF system and subjected to the static loading condition. Based on obtained experimental and numerical results following conclusions are listed:

(1). An analytical solution is proposed for investigating the equivalent mechanical properties of the composite bone-inspired structure. This function is defined in the PSO optimization algorithm to obtain unit cells with the highest and most optimal stiffnesses. Compressive simulation results demonstrated that initial peak force, plateau stress area, and energy absorption capacity increased significantly in optimized cellular structure and the unit cell with optimum stiffness has more mechanical potential to be employed in energy absorber instruments.

(2). VUSFLD subroutine was developed in numerical simulations to decrease mechanical properties in composite struts of the unit cell. According to numerical and experimental results, this simulation method has good agreements and the proposed model can predict the behaviour of cellular structures well. This can be useful in designing cellular structures and in reducing manufacturing costs.

(3). According to experimental tests and numerical simulation adding continuous glass fiber as

the second phase to PLA material the mechanical performance of the structures improved significantly. Based on the results energy absorption capacity increased by 250% in fiber-reinforced structures compared to un-reinforced structures.

References

[1] M. Sadeghzade, H. Gharehbaghi, and A. Farrokhabadi, "Experimental and analytical studies of mechanical properties of additively manufactured lattice structure based on octagonal bipyramid cubic unit cell," *Addit. Manuf.*, vol. 48, no. PB, p. 102403, 2021, doi: 10.1016/j.addma.2021.102403.

[2] B. Fan, Z. Xu, Y. Lin, and Z. Huang, "Mechanical properties of a novel two-phase hybrid plate-lattice metamaterial," *Mech. Adv. Mater. Struct.*, vol. 0, no. 0, pp. 1–12, 2022, doi: 10.1080/15376494.2022.2104974.

[3] A. Farrokhabadi, H. Gharehbaghi, H. Malekinejad, M. Sebghatollahi, Z. Noroozi, and H. Veisi, "Study of equivalent mechanical properties and energy absorption of composite honeycomb structures," *Int. J. Appl. Mech.*, Mar. 2023, doi: 10.1142/S1758825123500382.

[4] H. Gharehbaghi, M. Sadeghzade, and A. Farrokhabadi, "Introducing the new lattice structure based on the representative element double octagonal bipyramid," *Aerosp. Sci. Technol.*, vol. 121, p. 107383, 2022, doi: https://doi.org/10.1016/j.ast.2022.107383.

[5] E. Cuan-Urquizo *et al.*, "Elastic response of lattice arc structures fabricated using curved-layered fused deposition modeling," *Mech. Adv. Mater. Struct.*, vol. 28, no. 14, pp. 1498–1508, 2021, doi: 10.1080/15376494.2019.1682728.

[6] X. Zhou *et al.*, "Advances in 3D/4D printing of mechanical metamaterials: From manufacturing to applications," *Compos. Part B Eng.*, vol. 254, p. 110585, 2023, doi: https://doi.org/10.1016/j.compositesb.2023.110585.

[7] Z. Wang *et al.*, "3D printing of architectured epoxy-based composite lattices with exceptional strength and toughness," *Compos. Part B Eng.*, vol. 256, p. 110653, 2023, doi: https://doi.org/10.1016/j.compositesb.2023.110653.

[8] M. B. Francisco, J. L. J. Pereira, G. A. Oliver, L. R. Roque da Silva, S. S. Cunha, and G. F. Gomes, "A review on the energy absorption response and structural applications of auxetic structures," *Mech. Adv. Mater. Struct.*, vol. 29, no. 27, pp. 5823–5842, Nov. 2022, doi: 10.1080/15376494.2021.1966143.

[9] L. Bai, C.-T. Yi, X. Chen, Y. Sun, and J. Zhang, "Effective Design of the Graded Strut of BCC Lattice Structure for Improving Mechanical Properties," *Materials (Basel).*,

vol. 12, 2019.

[10] M. N. Uddin, H. T. N. Gandy, M. M. Rahman, and R. Asmatulu, “Adhesiveless honeycomb sandwich structures of prepreg carbon fiber composites for primary structural applications,” *Adv. Compos. Hybrid Mater.*, vol. 2, no. 2, pp. 339–350, 2019, doi: 10.1007/s42114-019-00096-6.

[11] L. Bai *et al.*, “Improved mechanical properties and energy absorption of Ti6Al4V laser powder bed fusion lattice structures using curving lattice struts,” *Mater. Des.*, vol. 211, p. 110140, 2021, doi: https://doi.org/10.1016/j.matdes.2021.110140.

[12] X. Wang, Y.-L. Chen, and L. Ma, “The manufacture and characterization of composite three-dimensional re-entrant auxetic cellular structures made from carbon fiber reinforced polymer,” *J. Compos. Mater.*, vol. 52, pp. 3265–3273, 2018.

[13] A. Ingrole, A. Hao, and R. Liang, “Design and modeling of auxetic and hybrid honeycomb structures for in-plane property enhancement,” *Mater. Des.*, vol. 117, pp. 72–83, 2017, doi: 10.1016/j.matdes.2016.12.067.

[14] H. Gharehbaghi, A. Farrokhabadi, and Z. Noroozi, “Introducing a new hybrid surface strut-based lattice structure with enhanced energy absorption capacity,” *Mech. Adv. Mater. Struct.*, vol. 0, no. 0, pp. 1–10, 2023, doi: 10.1080/15376494.2023.2167246.

[15] S. Okubo, Y. Yamauchi, and K. Kitazono, “Effects of random and controlled irregularity in strut lattice structure of PA12 on compression anisotropy,” *Addit. Manuf.*, vol. 63, p. 103385, 2023, doi: https://doi.org/10.1016/j.addma.2022.103385.

[16] A. Ghazlan, T. Nguyen, T. Ngo, S. Linforth, and V. T. Le, “Performance of a 3D printed cellular structure inspired by bone,” *Thin-Walled Struct.*, vol. 151, no. August 2019, p. 106713, 2020, doi: 10.1016/j.tws.2020.106713.

[17] A. Ghazlan, T. Ngo, T. Nguyen, S. Linforth, and T. Van Le, “Uncovering a high-performance bio-mimetic cellular structure from trabecular bone,” *Sci. Rep.*, vol. 10, no. 1, pp. 1–13, 2020, doi: 10.1038/s41598-020-70536-7.

[18] W. Zhang, S. Yin, T. X. Yu, and J. Xu, “Crushing resistance and energy absorption of pomelo peel inspired hierarchical honeycomb,” *Int. J. Impact Eng.*, vol. 125, no. November 2018, pp. 163–172, 2019, doi: 10.1016/j.ijimpeng.2018.11.014.

[19] N. S. Ha, T. M. Pham, T. T. Tran, H. Hao, and G. Lu, “Mechanical properties and energy absorption of bio-inspired hierarchical circular honeycomb,” *Compos. Part B Eng.*, vol. 236, p. 109818, 2022, doi: https://doi.org/10.1016/j.compositesb.2022.109818.

[20] M. Xu *et al.*, “In-plane compression behavior of hybrid honeycomb metastructures: Theoretical and experimental studies,” *Aerosp. Sci. Technol.*, vol. 106, p. 106081, 2020, doi: 10.1016/j.ast.2020.106081.

[21] R. Doodi and B. M. Gunji, “An experimental and numerical investigation on the performance of novel hybrid bio-inspired 3D printed lattice structures for stiffness and

energy absorption applications," *Mech. Adv. Mater. Struct.*, pp. 1–10, Mar. 2023, doi: 10.1080/15376494.2023.2188324.

[22] Q. Lu, D. Qi, Y. Li, D. Xiao, and W. Wu, "Impact energy absorption performances of ordinary and hierarchical chiral structures," *Thin-Walled Struct.*, vol. 140, no. March, pp. 495–505, 2019, doi: 10.1016/j.tws.2019.04.008.

[23] D. Zhang, Q. Fei, and P. Zhang, "In–plane dynamic crushing behavior and energy absorption of honeycombs with a novel type of multi-cells," *Thin-Walled Struct.*, vol. 117, no. September 2016, pp. 199–210, 2017, doi: 10.1016/j.tws.2017.03.028.

[24] D. Li, W. Liao, N. Dai, and Y. M. Xie, "Absorption of Sheet-Based and Strut-Based Gyroid," *Materials (Basel).*, 2019.

[25] S. Higuera, R. Miralbes, and D. Ranz, "Mechanical properties and energy–absorption capabilities of thermoplastic sheet gyroid structures," *Mech. Adv. Mater. Struct.*, vol. 29, no. 25, pp. 4110–4124, Oct. 2022, doi: 10.1080/15376494.2021.1919803.

[26] X. Wang, T. Gao, C. Shi, Y. Zhou, Z. Li, and Z. Wang, "Effect of geometric configuration on compression behavior of 3D-printed polymeric triply periodic minimal surface sheets," *Mech. Adv. Mater. Struct.*, pp. 1–11, Apr. 2022, doi: 10.1080/15376494.2022.2053906.

[27] A. Forés-Garriga, G. Gómez-Gras, and M. A. Pérez, "Additively manufactured three-dimensional lightweight cellular solids: Experimental and numerical analysis," *Mater. Des.*, vol. 226, p. 111641, 2023, doi: https://doi.org/10.1016/j.matdes.2023.111641.

[28] H. Rahman, E. Yarali, A. Zolfagharian, A. Serjouei, and M. Bodaghi, "Energy absorption and mechanical performance of functionally graded soft–hard lattice structures," *Materials (Basel).*, vol. 14, no. 6, 2021, doi: 10.3390/ma14061366.

[29] Z. Huang, B. Li, L. Ma, and Y. Li, "Mechanical properties and energy absorption performance of bio-inspired dual architecture phase lattice structures," *Mech. Adv. Mater. Struct.*, pp. 1–11, Mar. 2022, doi: 10.1080/15376494.2022.2045654.

[30] V. Rajendra Boopathy, A. Sriraman, and G. Arumaikkannu, "Energy absorbing capability of additive manufactured multi-material honeycomb structure," *Rapid Prototyp. J.*, vol. 25, no. 3, pp. 623–629, 2019, doi: 10.1108/RPJ-03-2018-0066.

[31] C. Quan, B. Han, Z. Hou, Q. Zhang, X. Tian, and T. J. Lu, "3D Printed Continuous Fiber Reinforced Composite Auxetic Honeycomb Structures," *Compos. Part B Eng.*, vol. 187, p. 107858, 2020, doi: 10.1016/j.compositesb.2020.107858.

[32] H. Veisi and A. Farrokhabadi, "Investigation of the equivalent material properties and failure stress of the re-entrant composite lattice structures using an analytical model," *Compos. Struct.*, vol. 257, no. September, p. 113161, 2021, doi: 10.1016/j.compstruct.2020.113161.

[33] A. Farrokhabadi, H. Veisi, H. Gharehbaghi, J. Montesano, A. H. Behravesh, and S. K. Hedayati, "Investigation of the energy absorption capacity of foam-filled 3D-printed

glass fiber reinforced thermoplastic auxetic honeycomb structures," *Mech. Adv. Mater. Struct.*, pp. 1–12, Feb. 2022, doi: 10.1080/15376494.2021.2023919.

[34] T. Liu, C. Chen, and Y. Cheng, "Mechanical characteristics and foam filling enhancement mechanism of polymeric periodic hybrid structures under uniaxial compression," *Mater. Des.*, vol. 227, p. 111762, 2023, doi: https://doi.org/10.1016/j.matdes.2023.111762.

[35] A. Farrokhabadi, M. M. Ashrafian, H. Gharehbaghi, and R. Nazari, "Evaluation of the equivalent mechanical properties in a novel composite cruciform honeycomb using analytical and numerical methods," *Compos. Struct.*, vol. 275, p. 114410, 2021, doi: https://doi.org/10.1016/j.compstruct.2021.114410.

[36] A. Farrokhabadi, M. M. Ashrafian, and M. Fotouhi, "Design and characterization of an orthotropic accordion cellular honeycomb as one-dimensional morphing structures with enhanced properties," *J. Sandw. Struct. Mater.*, p. 10996362211070248, Jan. 2022, doi: 10.1177/10996362211070249.

[37] W. Hao, Y. Liu, T. Wang, G. Guo, H. Chen, and D. Fang, "Failure analysis of 3D printed glass fiber/PA12 composite lattice structures using DIC," *Compos. Struct.*, vol. 225, no. May, p. 111192, 2019, doi: 10.1016/j.compstruct.2019.111192.

[38] Z. Xin, X. Zhang, Y. Duan, and W. Xu, "Nacre-inspired design of CFRP composite for improved energy absorption properties," *Compos. Struct.*, vol. 184, pp. 102–109, 2018, doi: 10.1016/j.compstruct.2017.09.075.

[39] C. Hu, J. Dong, J. Luo, Q. H. Qin, and G. Sun, "3D printing of chiral carbon fiber reinforced polylactic acid composites with negative Poisson's ratios," *Compos. Part B Eng.*, vol. 201, no. June, p. 108400, 2020, doi: 10.1016/j.compositesb.2020.108400.

[40] J. Plocher and A. Panesar, "Effect of density and unit cell size grading on the stiffness and energy absorption of short fibre-reinforced functionally graded lattice structures," *Addit. Manuf.*, vol. 33, no. March, 2020, doi: 10.1016/j.addma.2020.101171.

[41] K. Günaydın, C. Rea, and Z. Kazancı, "Energy absorption enhancement of additively manufactured hexagonal and re-entrant (auxetic) lattice structures by using multi-material reinforcements," *Addit. Manuf.*, vol. 59, p. 103076, 2022, doi: https://doi.org/10.1016/j.addma.2022.103076.

[42] F. Ghorbani, H. Gharehbaghi, A. Farrokhabadi, and A. Bolouri, "Investigation of the equivalent mechanical properties of the bone-inspired composite cellular structure: Analytical, numerical and experimental approaches," *Compos. Struct.*, vol. 309, no. January, p. 116720, 2023, doi: 10.1016/j.compstruct.2023.116720.

[43] Q. Bai, "Analysis of Particle Swarm Optimization Algorithm," *Comput. Inf. Sci.*, vol. 3, no. 1, 2010, doi: 10.5539/cis.v3n1p180.

[44] D. Wang, D. Tan, and L. Liu, "Particle swarm optimization algorithm : an overview," *Soft Comput.*, 2017, doi: 10.1007/s00500-016-2474-6.

[45] B. Akhoundi, A. H. Behravesh, and A. Bagheri Saed, “Improving mechanical properties of continuous fiber-reinforced thermoplastic composites produced by FDM 3D printer,” *J. Reinf. Plast. Compos.*, vol. 38, no. 3, pp. 99–116, 2019, doi: 10.1177/0731684418807300.

[46] C. Qi, F. Jiang, S. Yang, and A. Remennikov, “Multi-scale characterization of novel re-entrant circular auxetic honeycombs under quasi-static crushing,” *Thin-Walled Struct.*, vol. 169, no. July, p. 108314, 2021, doi: 10.1016/j.tws.2021.108314.